

Volatile Organic Compound Detection Using Insect Odorant-Receptor Functionalised Field-Effect Transistors

by

Eddyn Oswald Perkins Treacher

A thesis submitted in fulfilment of the
requirements of the degree of
Doctor of Philosophy in Physics
School of Physical and Chemical Sciences
Te Herenga Waka - Victoria University of Wellington

Aug 2023



Acknowledgements

69577

Rifat, Alex - vapour sensor
Erica Cassie - FET sensing setup
Rob Keyzers and Jennie Ramirez-Garcia - NMR spectra
Patricia Hunt - Computational chemistry

Abstract

This is a thesis skeleton written with quarto. Make a copy of this thesis repo and start to write!

Make a new paragraph by leaving a blank line.

Table of contents

Acknowledgements	1
Abstract	3
1. Introduction	7
2. Carbon Nanotube and Graphene Field-Effect Transistors	9
2.1. Ambipolar Field-Effect Transistors	9
2.1.1. Gating	9
2.1.2. Electrical Properties	9
3. Carbon Nanotube and Graphene Field-Effect Transistors as Biosensor Platforms	11
3.1. Carbon Nanotube Networks & Graphene as Biosensing Transducers	11
3.2. Biosensor Examples	11
3.2.1. Sensor Types	11
3.2.2. Sensor Functionalisation	11
3.2.3. Sensing Methods	11
3.3. Insect Odorant Receptors	11
4. Fabrication of Carbon Nanotube Network and Graphene Field-Effect Transistors	13
4.1. Deposition of Carbon Nanotubes	13
4.1.1. Solvent-Based	14
4.1.2. Surfactant-Based	14
4.2. Photolithography for Carbon Nanotube and Graphene Field-Effect Transistors	17
4.2.1. Alignment Markers	18
4.2.2. Channel Etching	19
4.2.3. Electrodes	19
4.2.4. Encapsulation	21
4.3. Characterisation via Fluorescence Microscopy	21
4.4. Characterisation via Atomic Force Microscopy	21
4.5. Electrical Characterisation	21

Table of contents

5. Functionalisation of Carbon Nanotubes and Graphene with Odorant Receptors	23
5.1. Linker molecules	23
5.1.1. 1-Pyrenebutanoic acid N-hydroxysuccinimide ester (PBASE) . . .	23
6. Results	27
7. Vapour Phase Sensing with Transistor Biosensors	29
7.1. Testing Vapour Delivery System	29
7.1.1. System Description	29
7.1.2. Temperature and Humidity Indicator	29
7.1.3. Photoionisation Detector	29
8. Summary	31
Appendices	31
A. Photolithography	33
A.1. AZ® 1518 photoresist	35
A.2. AZ® nLOF 2020 photoresist	35
A.3. SU8-2150 photoresist	36
B. Python Code for Data Analysis	37
C. Vapour Delivery System	39
C.1. Technical Notes	39
C.2. Future Improvements	39

1. Introduction

This is a book created from markdown and executable code.

See for additional discussion of literate programming.

[1] 2

2. Carbon Nanotube and Graphene Field-Effect Transistors

2.1. Ambipolar Field-Effect Transistors

2.1.1. Gating

Back-gating

Liquid-gating

2.1.2. Electrical Properties

3. Carbon Nanotube and Graphene Field-Effect Transistors as Biosensor Platforms

3.1. Carbon Nanotube Networks & Graphene as Biosensing Transducers

3.2. Biosensor Examples

3.2.1. Sensor Types

3.2.2. Sensor Functionalisation

3.2.3. Sensing Methods

Aqueous Environment

Vapour Environment

3.3. Insect Odorant Receptors

4. Fabrication of Carbon Nanotube Network and Graphene Field-Effect Transistors

This chapter discusses the fabrication processes for both the carbon nanotube network and graphene transistors. Experimental optimisation of the transducer element is critical for biosensor work, and large numbers of transducers were required for testing various biosensor functionalisation processes. Therefore, these processes were developed to rapidly fabricate devices with reproducible device characteristics appropriate for biosensing work. Also outlined in this chapter are the characterisation techniques taken to test the quality and reproducibility of these fabrication processes.

The nitrogen ($\geq 99.99\%$) and oxygen (99.7%) used in fabrication work was supplied by BOC Limited New Zealand. Deionised (DI) water was taken from a Synergy® UV Water Purification System. The DI water had a measured conductivity of $(1.4 \pm 0.1) \mu\text{S cm}^{-1}$, compared to tap water with a measured conductivity of $(7.8 \pm 0.2) \mu\text{S cm}^{-1}$.

4.1. Deposition of Carbon Nanotubes

4-inch *p*-type (B-doped) silicon wafers with either a 100 nm or 300 nm SiO₂ layer (Wafer-Pro LLC) were used as the substrate for carbon nanotube network deposition. A 100 nm SiO₂ layer was the preferred option for the devices intended for backgated measurements. Before deposition of carbon nanotubes, the wafers were spin-coated with AZ® 1518 photoresist, placed photoresist-side down onto a cleanroom wipe, fixed in place using vacuum suction, then cleaved into quarters using a diamond-tipped scribe tool. For fabrication performed before June 2023, the protective photoresist layer was then removed by soaking the quarter-wafers in acetone for 15 minutes, then rinsed with isopropyl alcohol (IPA) and dried with N₂ gas. However, for complete removal of photoresist, we found it was necessary to flood expose the wafer with the Karl Suss Aligner for 1 min and then place it in AZ326 developer for 3 min, as discussed further in Section 4.3.

Carbon nanotubes were deposited before alignment markers photolithography on all wafers fabricated between Aug 2021-Feb 2023, while devices fabricated before Aug 2021 and after Feb 2023 had alignment markers photolithography performed before the deposition of carbon nanotubes. The process order was first switched in Aug 2021 as this

4. Fabrication of Carbon Nanotube Network and Graphene Field-Effect Transistors

order led to faster processing times. However, the order was switched back in Feb 2023 to minimise the exposure of carbon nanotubes to photolithographic chemical processes.

4.1.1. Solvent-Based

The solvent-based deposition process for the carbon nanotube network in the second fabrication protocol is as follows. 10 mg of 2-mercaptopurine (99%, Sigma-Aldrich) was dissolved in 1 ml ethanol by sonication until clear. Quarter wafers were sonicated in acetone for 3 min, then exposed to O₂ plasma at 100 W for at least 2 min in a small plasma cleaner (Plasma Etch, Inc., PE-50 Compact Benchtop Plasma Cleaning System) or reactive ion etcher (Oxford Instruments, Plasmalab® 80 Plus) under 300 mTorr pressure. The cleaned SiO₂/Si surface was then coated with 2-mercaptopurine for 10 minutes, rinsed with ethanol to remove residual 2-mercaptopurine, and then nitrogen dried. Meanwhile, 5 µg of 99% semiconducting carbon nanotube bucky paper (NanoIntegris, IsoNanotubes S-99) was dispersed in 10 mL of anhydrous 1,2-dichlorobenzene (Sigma Aldrich) by ultrasonication until no particles were visible to the naked eye. During this time, the ultrasonic bath temperature was kept between 20 - 30 °C or the buckypaper would not disperse successfully. The substrates were then placed into a dish with CNT-DCB suspension and left covered for 1 hour, dipped into ethanol for 10 min to remove residual solvent and any unattached carbon nanotube bundles, and then dried with nitrogen.

4.1.2. Surfactant-Based

Two different approaches were used to attach the surfactant-dispersed CNTs. In both approaches, the quarter wafers were rinsed with ultrapure deionised water (DI water), acetone and IPA before being placed into a reactive ion etcher (Oxford Instruments, Plasmalab 80 Plus) and exposed to O₂ plasma at 100 W for at least 2 min in a small plasma cleaner (Plasma Etch, Inc, PE-50 Compact Benchtop Plasma Cleaning System) or reactive ion etcher (Oxford Instruments, Plasmalab 80 Plus) under 300 mTorr pressure to make the surface hydrophilic. 1 mL of poly-L-lysine (PLL) was immediately deposited onto each quarter wafer and left for 5 minutes. Then, the quarter wafers were rinsed for 30 s with DI water and dried with N₂ gas. This process allows for the surface adhesion of semiconducting single carbon nanotubes suspended in surfactant.

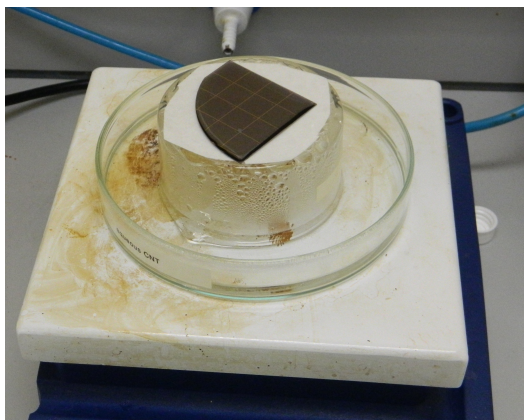
Simple Dropcasting

2 mL of IsoNanotubes-S 90% or 99% solution (NanoIntegris) was decanted into a small bottle and sonicated for 5 s to break up bundles of CNTs. An even spread of 400 µL CNT solution was placed in the centre of the PLL-functionalised quarter wafer, covered and left for 10 minutes. The CNT solution was then rinsed off with DI water and IPA, and then the quarter wafer was dried with N₂ gas. Next, the quarter wafer was annealed in a

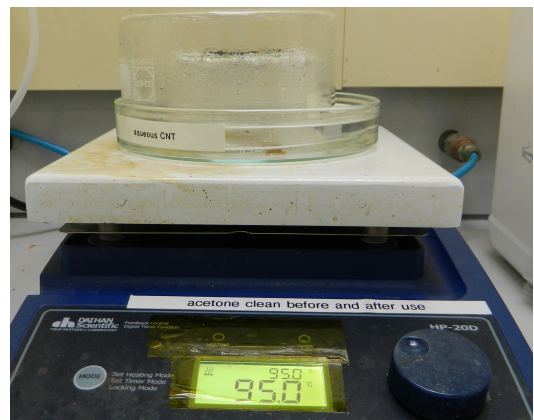
4.2. Photolithography for Carbon Nanotube and Graphene Field-Effect Transistors

vacuum oven at 150° C for 1 hour. This method would often lead to an inhomogeneous spread of CNTs across the quarter wafer surface, detailed further in section Section 4.4.

Steam-Assisted Method



(a) Steam method setup without steam cover



(b) Steam method setup with steam cover

Figure 4.1.: Photographs of steam-assisted method setup (top and side view).

2 mL of IsoNanotubes-S 90% or 99% solution (NanoIntegris) was decanted into a small bottle and burst-sonicated once (on then off again) to break up bundles of CNTs. 75 mL of 95° C water was then placed into a glass dish on a hotplate held at 95° C. After this, the PLL-functionalised quarter wafer was placed in the centre of an insulating surface on the same hotplate. The CNT dispersion was carefully spread across the surface of the wafer without spilling any over the wafer edges. The wafer on the insulating surface and glass dish were then left under the same cover for 2 minutes to expose the wafer to steam from the glass dish. The use of an insulating surface meant that the wafer and CNT dispersion were not heated from below while exposed to steam. The steam-assisted deposition setup is shown in Figure 4.1.

The CNT dispersion was then rinsed off the wafer with DI water, ethanol, acetone and IPA, and then the quarter wafer was dried with N₂ gas. As in the original method, the quarter wafer was then annealed in a vacuum oven at 150° C for 1 hour. This method gave an even spread of CNTs across the quarter wafer surface, leading to a greater consistency in performance between devices. Further details can be found in Section 4.4.

4. Fabrication of Carbon Nanotube Network and Graphene Field-Effect Transistors

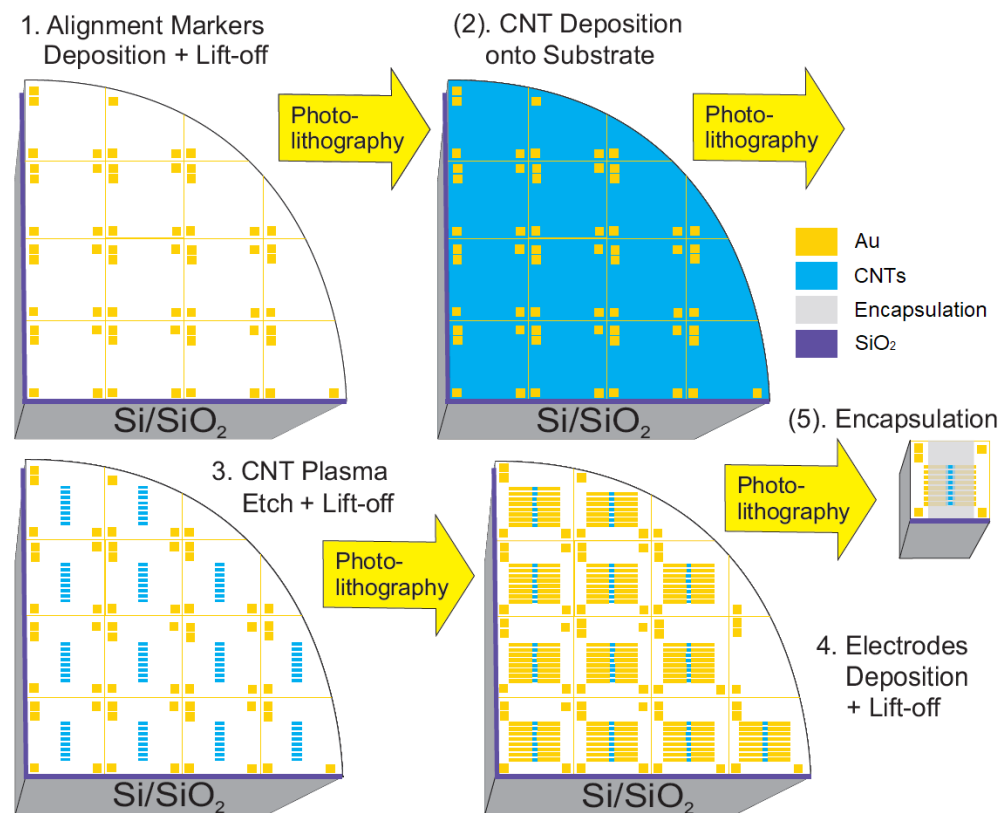


Figure 4.2.: The photolithographic processes used for fabrication of both carbon nanotube and graphene devices (graphene devices were fabricated individually for every step, step #2 skipped for graphene devices)

4.2. Photolithography for Carbon Nanotube and Graphene Field-Effect Transistors

Photolithography was used to define eight channel regions on each device and subsequently to define metal contacts for each of these channels. A schematic demonstrating these photolithography processes on a quarter wafer is shown in Figure 4.2.

Thermal evaporation was used when depositing chromium (Cr-plated tungsten rods, Kurt J. Lesker) and gold (Au wire, 99.99%, Regal Castings Ltd.), while electron beam evaporation was used when depositing titanium (Ti pieces, 99.99%, Kurt J. Lesker) and metal oxides (*e.g.* Al₂O₃ pieces, 99.99%, Kurt J. Lesker). Metal and metal oxide deposition was performed using an Angstrom Engineering Nexdep 200 Vacuum Deposition System. Deposition thickness was controlled using an Inficon Deposition Controller and electron beam power was provided by a Telemark TT-6 power supply. For metals, the chamber was initially evacuated to a pressure 5×10^{-6} mTorr, while for metal oxides the chamber was initially evacuated to a pressure below 1×10^{-5} mTorr. After evaporation, the chamber was cooled and vented with nitrogen.

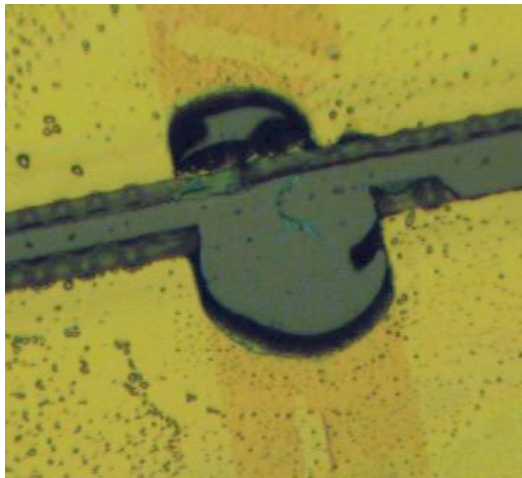
Carbon nanotube devices were fabricated using the quarter wafer substrates discussed in Section 4.1.

Graphene devices were fabricated using 300 nm SiO₂/p-type Si substrates covered with a monolayer of mechanically transferred CVD graphene (Advanced Chemical Supplier). This substrate was cleaved into equal-sized square chips before photolithography, with side length between 11.6 - 11.7 mm, subject to variability in wafer size. The same cleaving process outlined in Section 4.1 was used for cleaving the chips, but the photoresist was not rinsed off after cleaving. Devices were exposed to a brief burst of N₂ gas to remove any dust from the cleaving process from the surface of devices. When not being used in photolithography, devices were stored in a vacuum desiccator to prevent the quality of the graphene deteriorating with exposure to air over time.

Dimethyl sulfoxide (DMSO) was sometimes used in lift-off processes instead of acetone between Jul 2021 and Feb 2023 because of its effectiveness as a photoresist stripping agent. However, it was abandoned due to some indications it was too aggressive for the devices being fabricated, as shown in Figure 4.3 and also as detailed in Section 4.4. It is possible that heat from the electrodes deposition sometimes crosslinked residual photoresist on the nanomaterial, and then during lift-off was removed aggressively together with any attached nanomaterial by the DMSO. However, it is also possible that prolonged exposure to DMSO alone was sufficient to detach nanomaterial from the substrate. Therefore, acetone was the preferred agent for lift-off despite being a less efficient stripping agent than DMSO.

From Jul 2023 onwards, after each photolithography step, quarter wafers/chips were flood exposed to UV light for 1 min and then placed in AZ326 developer for 3 min to ensure complete removal of photoresist residue (discussed in Section 4.3).

4. Fabrication of Carbon Nanotube Network and Graphene Field-Effect Transistors



(a) Damage to gold electrode in channel region after DMSO lift-off



(b) Damage to graphene (blue region) after DMSO lift-off

Figure 4.3.: Lift-off with dimethyl sulfoxide sometimes led to damage to regions where nanomaterials were present.

4.2.1. Alignment Markers

Metal alignment markers were deposited in order to accurately align the device channels with device electrodes in subsequent photolithography steps. These alignment markers were asymmetric to indicate the orientation of the device for subsequent photolithography steps and electrical characterisation. In later discussion, channel 1 is defined as the channel placed closest to the large, double square alignment marker.

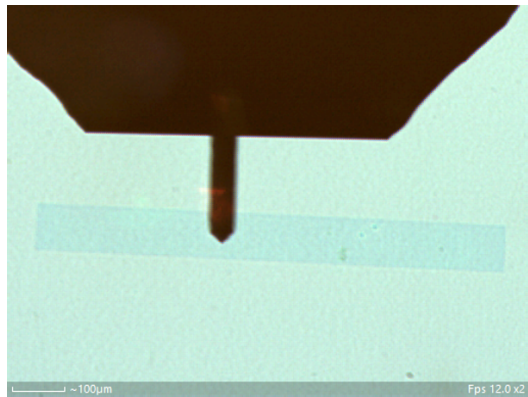
For carbon nanotube quarter wafers, alignment markers were deposited either directly before or after carbon nanotube deposition (see Section 4.1 for discussion). For graphene devices, alignment markers were deposited directly after cleaving using the protective photoresist layer spincoated prior to cleaving. AZ® 1518 was used for alignment marker photolithography.

For carbon nanotube devices made before Jun 2022, chromium was used as an adhesive layer for gold, while for all graphene devices and carbon nanotube devices made after Jun 2022, titanium was used as the adhesive layer. For chromium/gold depositions, a nominal 10 nm of chromium was deposited followed by a nominal 100 nm Au layer. For titanium/gold depositions, a nominal 10-20 nm of titanium was deposited followed by a nominal 50 nm Au layer (for independent measurements of metal layer thickness, see Section 4.2.3). Devices were then soaked in acetone for at least 2 hours for photoresist lift-off, washed in IPA and dried with nitrogen. The use of titanium gave rise to a cleaner lift-off and improved gold adhesion. Using a relatively thin gold layer (50 nm nominal instead of 100 nm) proved to still be clearly visible but to a cleaner lift-off.

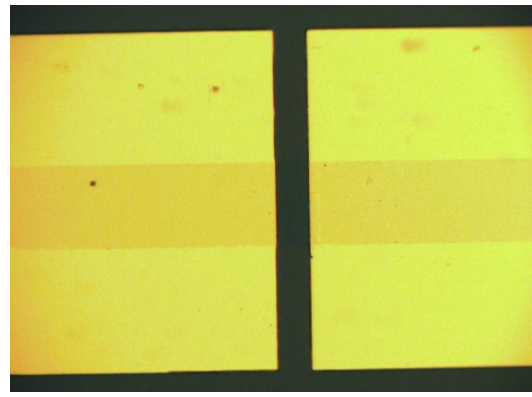
4.2. Photolithography for Carbon Nanotube and Graphene Field-Effect Transistors

4.2.2. Channel Etching

Eight channel features, each 1000 μm in length and 100 μm in width with a pitch of 1200 μm , were patterned using AZ® 1518 photolithography on each carbon nanotube or graphene-covered substrate. Unwanted nanomaterial not covered with photoresist was then etched away with 200 W oxygen plasma at 600 mTorr using a reactive ion etcher or RIE (Plasmalab® 80 Plus, Oxford Instruments). The etch time was 3 minutes for carbon nanotube quarter wafers, and 1 minute for graphene chips. The protective photoresist was then removed by soaking in acetone for at least 5 minutes.



(a) Graphene channel after photolithographically defined plasma etch



(b) Graphene channel after photolithographically defined electrodes deposition and liftoff

Figure 4.4.: Microscope images of a graphene channel after plasma etch and electrodes photolithography steps.

4.2.3. Electrodes

The source and drain electrodes for each channel were patterned using photolithography with either AZ® 1518 photoresist (pre-Mar 2023) or AZ® nLOF 2020 photoresist (post-Mar 2023). To ensure the patterned areas were clean of photoresist after development, they were exposed to O₂ plasma at 50 W for 2-5 s or at 20 W for 25 s in the PE-50 plasma cleaner (Plasma Etch, Inc.) directly before being loaded into the thermal evaporator.

As with the alignment markers deposition (see Section 4.2.1), before Jun 2022 chromium was used for the gold adhesive layer, and after Jun 2022 titanium was used. A 20 nm nominal titanium layer instead of 10 nm nominal was found to give better electrode adhesion, and devices after Feb 2023 were made using this thicker adhesion layer. Good electronic contact could be made with electrodes with a nominal gold layer thickness of 60-100 nm (see Section 4.5), and a Au layer nominally 100 nm thick was most commonly used.

4. Fabrication of Carbon Nanotube Network and Graphene Field-Effect Transistors

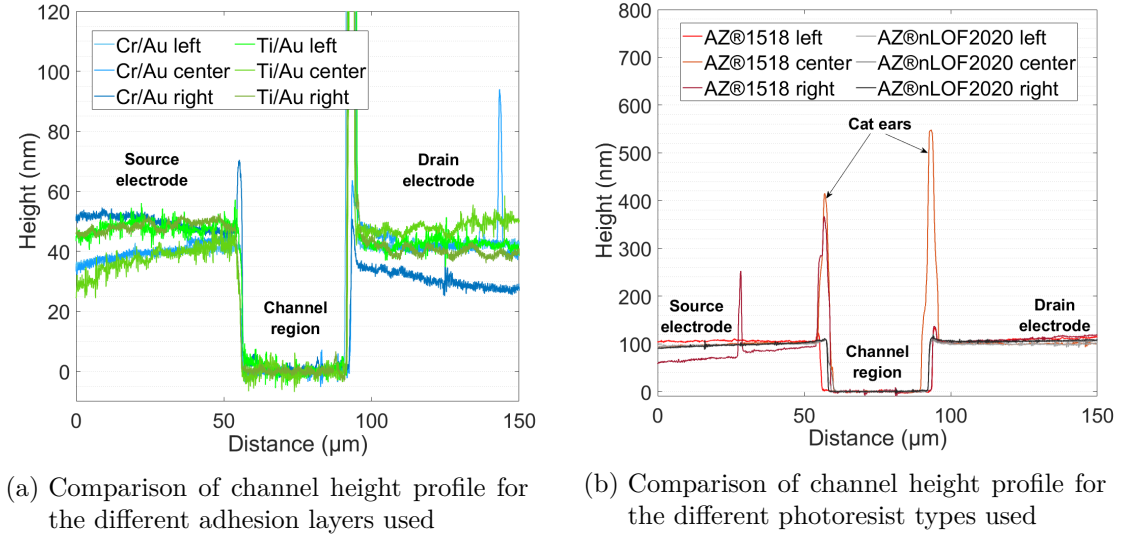


Figure 4.5.: Dektat height profiles taken between the source and drain electrodes across a channel from various quarter wafers with electrodes deposited using different approaches. For each quarter wafer, the profiles of three different channels are shown, selected from different locations across the quarter wafer surface.

Example height profiles of chromium layer channels and a titanium layer channels taken using a Veeco Dektat 150 profiler are shown in Figure 4.5a. AZ® 1518 photoresist was used here for photolithographic patterning. A 10 nm adhesion layer and 100 nm Au layer were used for both depositions to ensure a consistent comparison. From Figure 4.5a, we find an measured Cr/Au electrode height of 42 ± 1 nm and an measured Ti/Au electrode height of 48 ± 2 nm, slightly less than half the respective heights stated on the Inficon Deposition Controller.

Although using AZ® nLOF 2020 photolithography involves more processing steps, it gave rise to more cleanly-defined electrodes with a more consistent height profile. Often electrodes deposition using AZ® 1518 photoresist would lead to sharp vertical spikes along the edge of the electrode. These edge spikes or “cat ears” could partially or fully protrude through thin encapsulation materials such as SU8 and Al₂O₃, leading to significant leakage currents from the electrodes into the FET top gate. This effect is due to the profile of positive resists being suboptimal for lift-off processes, as discussed in Appendix A.

The height profiles corresponding to a wafer with electrodes fabricated using AZ® 1518 and to a wafer with electrodes fabricated using AZ® nLOF 2020 are shown in Figure 4.5b. A 20 nm titanium adhesion layer and 100 nm Au layer were used for both depositions to ensure a consistent comparison, resulting in a measured electrode height of 103 ± 2 nm for both wafers. The wafer which used AZ® nLOF 2020 photoresist clearly has a more consistent electrode height profile across the wafer surface than the wafer which

4.3. Characterisation via Fluorescence Microscopy

used AZ® 1518 resist. The measured edge features for the AZ® 1518 resist electrodes vary in size from 20 nm to 450 nm above the bulk electrode surface, whereas the edge features for the AZ® nLOF 2020 resist do not exceed 14 nm in height.

4.2.4. Encapsulation

Several different approaches were used for the encapsulation, or contact protection, of devices. The encapsulation of graphene and carbon-nanotube transistors for biosensing is essential to passivate the electrodes and ensure only the nanomaterial region is active during biosensing, as discussed in Section 3.2.3.

Before encapsulation photolithography the carbon-nanotube network quarter wafers were cleaved into individual 12 mm x 12 mm chips, using the cleaving process outlined in Section 4.1. Cleaving the devices at this step simplified mask alignment and ensured consistent thickness across photoresist encapsulated devices.

Photoresist encapsulation

Two types of photoresist were trialled for encapsulation, AZ® 1518 and SU8-2150.

Dielectric encapsulation

4.3. Characterisation via Fluorescence Microscopy

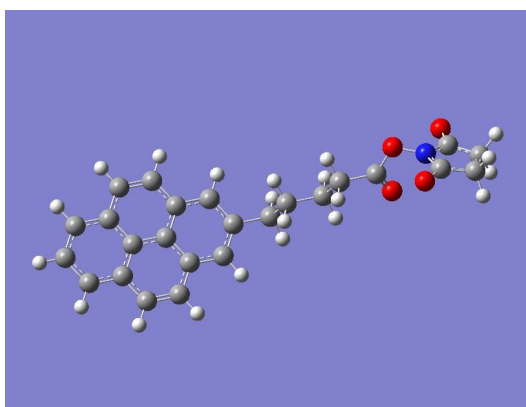
4.4. Characterisation via Atomic Force Microscopy

4.5. Electrical Characterisation

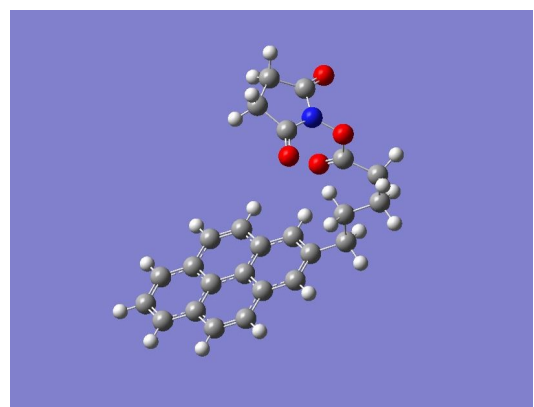
5. Functionalisation of Carbon Nanotubes and Graphene with Odorant Receptors

5.1. Linker molecules

5.1.1. 1-Pyrenebutanoic acid N-hydroxysuccinimide ester (PBASE)



(a) Hartree-Fock energy: -3427728.67 kJ/mol
(9 s.f.)



(b) Hartree-Fock energy: -3427729.66 kJ/mol
(9 s.f.)

Figure 5.1.: Two conformations of PBASE molecule with geometry optimised via *ab initio* calculation (computed using Gaussian 16 [1]). The difference between computed Hartree-Fock energies is 1.0 kJ/mol, small enough that the existence of both molecular conformations is physically possible.

1-Pyrenebutanoic acid N-hydroxysuccinimide ester (variously known commercially and in the literature as 1-Pyrenebutyric acid N-hydroxysuccinimide ester, PBASE, PBSE, PASE, Pyr-NHS, PyBASE, PANHS) is a aromatic, bifunctional molecule commonly used for tethering biomolecules to the carbon rings of graphene and carbon nanotubes. The optimised molecular structure of PBASE is shown in Figure 5.1.

The non-covalent functionalisation of proteins onto a single-walled carbon nanotube using PBASE was first reported by Chen *et al.* in 2001 [2]. Two methods for protein functionalisation and immobilisation were successfully used, with the only differences being the solvent used to dissolve the PBASE powder (DMF, methanol) and the final

5. Functionalisation of Carbon Nanotubes and Graphene with Odorant Receptors

concentration of the resulting solutions (6 mM, 1 mM respectively). The lower concentration may have been used for PBASE in methanol as PBASE powder appears to dissolve poorly in methanol at higher concentrations. Cella *et al.*, Campos *et al.*, Zheng *et al.* and Ohno *et al.* all directly cite Chen *et al.* when discussing functionalisation with PBASE [3]–[6]. Other groups using PBASE for graphene or carbon nanotube functionalisation do not explicitly reference Chen *et al.* in their methodology, but it is apparent they often draw on one of these two original methods. This common ancestry becomes apparent from the high frequency of methods detailing the use of 6 mM PBASE in DMF and 1 mM PBASE in methanol, as seen in Table 5.1.

However, despite this shared heritage, it is also apparent from Table 5.1 that there is a large degree of variation in the methods used for PBASE functionalisation. Various electrical characterisation, microscopy and spectroscopy techniques have been used to demonstrate successful functionalisation. However, there has historically been little justification provided for the exact parameters used in the procedure. As noted by Zhen *et al.* and Hinnemo *et al.*, there is more generally a lack of systematic research into formation of pyrene-derivative monolayers on graphene and other carbon nanomaterials, despite the wide use of this chemistry in the literature [7], [8].

We purchased PBASE from two suppliers, Sigma-Aldrich and Setareh Biotech. Sigma recommends DMF and methanol as suitable solvents for dissolving PBASE alongside chloroform and DMSO. Setareh Biotech indicates methanol can be used for dissolving PBASE. The two suppliers have conflicting information for suitable storage of PBASE, with Sigma recommending room temperature storage while Setareh Biotech recommends storage of -5 to -30°C and protection from light and moisture. Figure 5.2 compares the shapes of NMR spectra of PBASE from each supplier dissolved in DMSO, alongside a blank DMSO spectrum.

5.1. Linker molecules

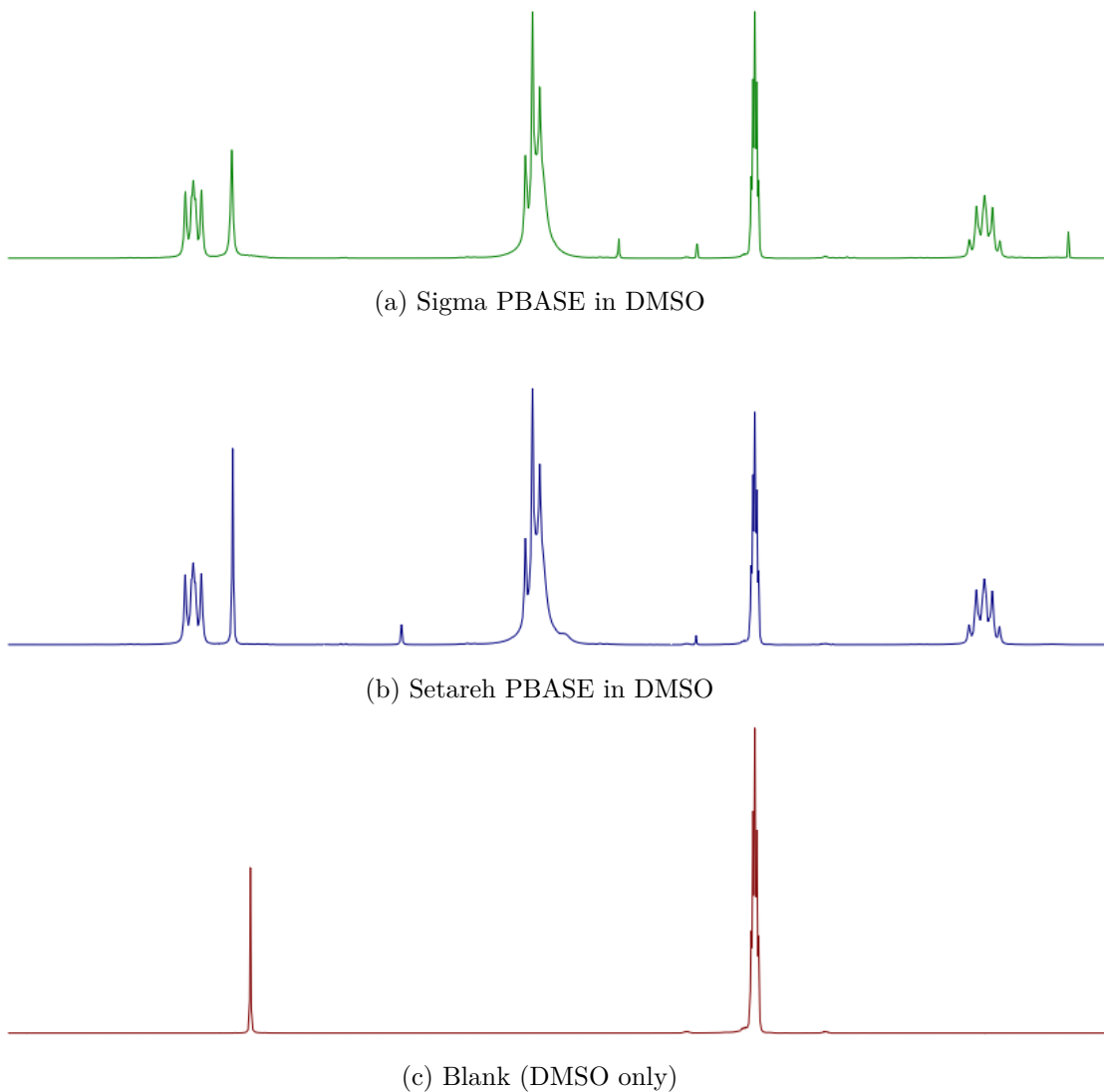


Figure 5.2.: Comparison of NMR spectrum profiles (arbitrary units)

5. Functionalisation of Carbon Nanotubes and Graphene with Odorant Receptors

Table 5.1.: Comparison of PBASE functionalisation processes used for immobilisation of proteins and aptamers onto liquid-gated CNTFET and graphene FET sensors

Solvent	Channel	Conc. (mM)	Incubation type	Time (hr)	Rinse steps	References	
DMF	CNTs	5	Immersed	1	PBS	Maehashi <i>et al.</i> [9]	
		6	Immersed	1	DMF, PBS	García-Aljaro <i>et al.</i> [10]	
		6	Immersed	1	DMF	Chen <i>et al.</i> [2]	
		6	Immersed	1	DMF	Cella <i>et al.</i> [3]	
		6	Immersed	1	DMF	Das <i>et al.</i> [11]	
	Graphene	-	-	2	DMF	Kwong Hong Tsang <i>et al.</i> [12]	
		-	-	20	-	Wiedman <i>et al.</i> [13]	
		0.2	Immersed	20	DMF, IPA, DI water	Gao <i>et al.</i> [14]	
		1	100 μ L droplet	6	DMF, IPA, DI water	Nekrasov <i>et al.</i> [15]	
		5	Immersed	1	DMF, DI water	Hwang <i>et al.</i> [16]	
2-Methoxyethanol	Graphene	6	6 μ L droplet	2	DMF, DI water	Nur Nasufiya <i>et al.</i> [17]	
		10	10 μ L droplet	2	DMF, DI water	Campos <i>et al.</i> [4]	
		10	Immersed	2	DMF, PBS	Kuscu <i>et al.</i> [18]	
		10	Immersed	1	DMF	Xu <i>et al.</i> [19]	
		10	Immersed	12	DMF, ethanol, DI water	Khan <i>et al.</i> [20]	
	Methanol	1	Immersed	1	DI water	Ono <i>et al.</i> [21]	
		CNTs	1	Immersed	1	Methanol, DI water	Zheng <i>et al.</i> [5]
		1	Immersed	2	Methanol	Kim <i>et al.</i> [22]	
		Graphene	5	Immersed	2	-	Sethi <i>et al.</i> [23]
		5	Immersed	1	Methanol, PBS	Ohno <i>et al.</i> [6]	
DMSO	CNTs	10	-	1	DI water	Lopez <i>et al.</i> [24]	
		10	Immersed	1	PBS	Strack <i>et al.</i> [25]	

6. Results

What I found out.

See for more detailed results

7. Vapour Phase Sensing with Transistor Biosensors

7.1. Testing Vapour Delivery System

7.1.1. System Description

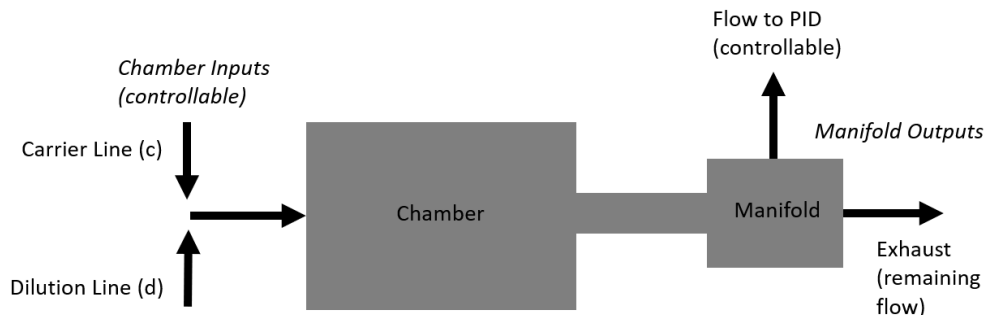


Figure 7.1.: Vapour Delivery System - Schematic of device chamber and manifold

7.1.2. Temperature and Humidity Indicator

7.1.3. Photoionisation Detector

Bubbling Vapour

First year report: ““First, a 200 sccm flow of N₂ gas was sent through the dilution line to the device chamber until 1000 s. Then, the flow controller three-way valves were manually adjusted so that the same 200 sccm flow was directed through 50 mL of EtOH analyte in the carrier line. This continued until 2200 s, where the valves were again manually adjusted so that 200 sccm clean N₂ again flowed through the device chamber. The resulting current across the device channel was monitored over this time, and is shown in Figure 19. A response to EtOH exposure and removal is visible.””

8. Summary

In summary, this book has no content whatsoever.

[1] 2

A. Photolithography

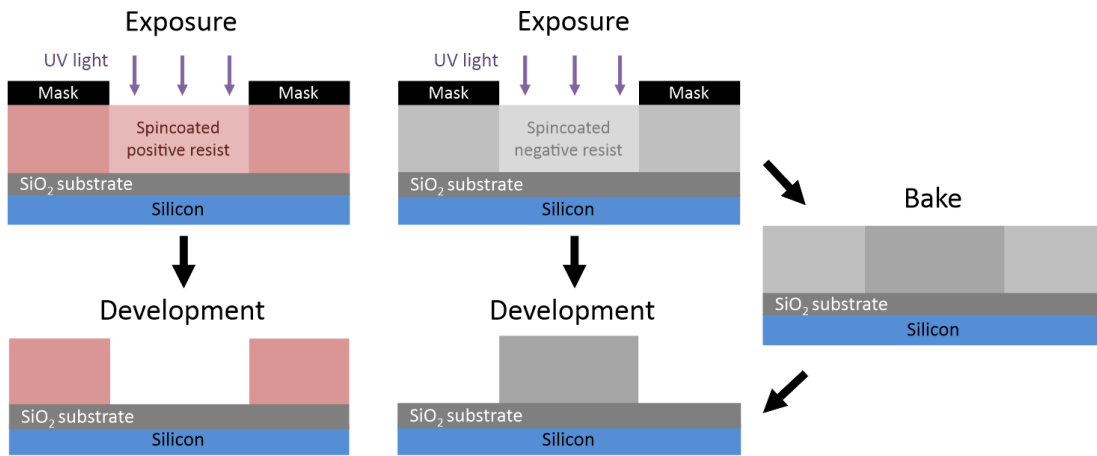


Figure A.1.: A side-view comparison of generic photolithography processes for positive and negative resists in the ideal case. Photolithography with a positive resist requires a single softbake step before exposure, while for negative resists a second baking step is required after exposure (Thicknesses shown not to scale).

This section details some of the standard photolithography procedures used in the device fabrication processes detailed in Chapter 4. Photoresists, also referred to here as “resists”, are UV light-sensitive polymeric resins used for photolithography. Both positive and negative photoresists were used in various fabrication processes. Positive resists are made soluble in alkalines by UV light exposure, meaning exposed areas are removed in the development process. Conversely, negative resists are cross-linked by exposure and a post-exposure bake step. The unexposed areas of the negative resist are then removed in the development process [26]. Figure A.1 gives a visual representation of these differences.

The specific photoresist selected for photolithography depends on the specific use case. The types used in this thesis are positive and negative AZ® photoresists (AZ® 1518, Microchemicals GmbH; AZ® nLOF 2020, Microchemicals GmbH) and SU-8 (SU8-2150, Kayaku Advanced Materials, formerly Microchem). The AZ® resists used here have a minimum film thickness of $1.5 \mu\text{m}$ [26], while the SU8-2150 has a minimum film thickness of $0.5 \mu\text{m}$ [27]. Positive resists which have not been thermally crosslinked will soften at higher temperatures ($\gtrsim 100^\circ\text{C}$ for AZ® 1518), leading to a rounded profile. This is not

A. Photolithography

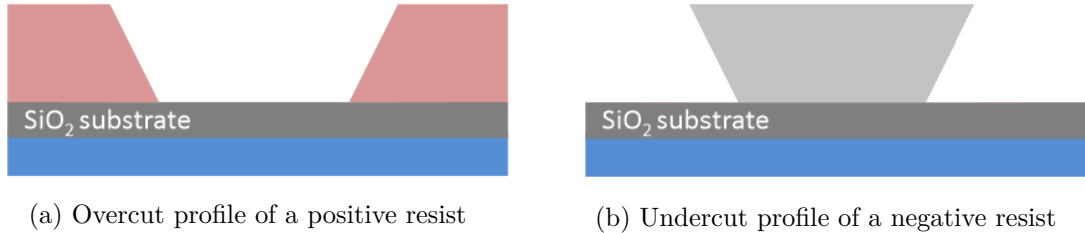


Figure A.2.: Two different resist profiles seen for different types of photoresist. The undercut profile is ideal for thin-film metal deposition and subsequent patterned removal, known as “lift-off”.

the case for negative resists, which are more thermally stable [26]. Each resist therefore has a different cross-section profile, as shown in Figure A.2.

If metal deposition is performed on a positive resist, some metal can collect on the outwardly-sloped sidewalls of the resist (see Figure A.2) which forms significant spikes on the edges of the deposited metal upon lift-off. On the other hand, metal cannot collect on top of the inwardly-sloped negative profile sidewalls, which avoids the formation of large edge spikes. Therefore, the negative resist profile is more suited to metal or metal oxide deposition and lift-off processes, though the process is more sensitive to human error due to requiring more processing steps than positive resist [26]. Finally, when it is suitably processed SU-8 is considered to be more biocompatible than other photoresists. It is especially biocompatible when chemically modified via processes such as isopropanol sonication and O₂ plasma treatment [28].

All photolithographic exposure was performed on a Karl Suss MJB3 Contact Aligner with a USHIO super-high pressure 350 W mercury lamp (USH-350DS, Japan). When performing lithography, the intensity reading from the aligner was 20.8 - 24.2 mW/cm² (Note however that an external photometer reading at 400 nm found an intensity output of 17.2 mW/cm² when the aligner read 21.0 mW/cm²).

In general, photolithography procedures should be performed under yellow lighting, as light wavelengths from 320-450 nm can promote reactions in the photoresist used. Aging of photoresist over time can also significantly affect the photolithography process, and therefore all processes should be re-optimised regularly over time to give the desired result [26]. The range in processing times for some steps of the processes used here are largely due to the effects of aging on the photoresist.

The step-by-step processes for each resist are detailed in the subsequent sections.

A.1. AZ® 1518 photoresist

1. Spincoat at a final speed of 4000 rotations per minute (rpm) for 1 minute, with an initial acceleration of 500 rpm/s (notes: clean the substrate with acetone, isopropanol (IPA) and nitrogen before spincoating; use only the minimum amount of photoresist required to fully cover the wafer surface; avoid any gaps or bubbles in the photoresist).
2. Softbake 2-4 minutes at 95°C on the hotplate (2 min for individual devices, 4 min for a quarter wafer)
3. Mask expose for 10-12 s (note: clean mask with acetone/IPA and N₂ dry before use)
4. Develop with 3 parts AZ® 326 (2.38 % TMAH metal-ion free developer, Microchemicals GmbH) in 1 part deionised (DI) water for 30-45 s (note: rinse for 10-15 s in one development solution, then perform the rest of the development in clean developer for a cleaner profile)
5. Rinse device for 30 s in DI water to remove excess developer, then dry under nitrogen

A.2. AZ® nLOF 2020 photoresist

1. Spincoat at final speed of 3000 rotations per minute (rpm) for 1 minute, with an initial acceleration of 500 rpm/s (notes: clean the substrate with acetone, isopropanol (IPA) and nitrogen before spincoating; avoid any gaps or bubbles in the photoresist)
2. Softbake for precisely 60 s at 110°C on the hotplate
3. Mask expose for 2.7-3 s (note: clean mask with acetone/IPA and N₂ dry before use)
4. Post-exposure bake for precisely 60 s at 110°C on the hotplate to cross-link exposed resist
5. Develop with 3 parts AZ® 326 in 1 part DI water for 60-70 s (note: rinse for 30 s in one development solution, then perform the rest of the development in clean developer for a cleaner profile)
6. Rinse device for 30 s in DI water to remove excess developer, then dry under nitrogen

A. Photolithography

A.3. SU8-2150 photoresist

1. SU-8 was diluted in cyclopentanone until viscosity was low enough to spincoat on substrate and then sonicated at 50°C for 3-4 hours (Note: The dilution ratio used was ~1 part SU-8 to 5 parts cyclopentanone. However, the age of the SU-8 may mean that significant evaporation had occurred prior to use, and the amount of SU-8 actually present is underrepresented by this ratio)
2. Spincoat first with a final speed of 500 rpm (acceleration 500 rpm/s) for 10 seconds, followed by spincoating at 4000 rpm (acceleration 7500 rpm/s) for 40 s.
3. Softbake for 10 minutes at 95°C on the hotplate
4. Mask expose for 6-8 s (note: clean mask with acetone/IPA and N₂ dry before use)
5. Post-exposure bake for 10 minutes at 95°C on the hotplate to cross-link exposed resist
6. Develop with SU-8 developer (Kayaku Advanced Materials, formerly Microchem) for 10-15 s, then clean in IPA for 30 s, repeat this step once then dry under nitrogen

B. Python Code for Data Analysis

C. Vapour Delivery System

C.1. Technical Notes

Two LabView Virtual Instruments (VIs) were adapted from pre-existing VIs for operating the mass flow controllers and monitoring vapour flow into the device chamber, as well as monitoring temperature and humidity in the vapour delivery system's manifold. These VIs were named “ ” A third VI was developed in parallel which combined the first two Virtual Instruments, alongside allowing the sequence of values to control the mass flow controllers.

From Honours report: “ ” Figure 12 gives the right side of the front panel of the LabView VI sample with vapour.VI, which lets us preset an autonomously-performed vapour sensing sequence. Each row in each array module corresponds to a different step in this sequence. The ‘howManySteps’ module lets us set how many of these steps are performed. The ‘Durations Array’ module determines the length of time in seconds each step is performed over. The ‘Carrier Flows Array’ and ‘Dilution Flows Array’ modules let us set the carrier flow and dilution flow, respectively, in standard cubic centimetres per minute (sccm) through the gas rig at each step. The carrier flow pushes analyte vapour into the vapour-sensing device chamber, while dilution flow is used to modify the flow behaviour of the analyte vapour entering the chamber. The vapour sensing sequence as depicted in Figure 12 was used for all vapour sensing runs in this investigation. At the end of the sequence, the data collected about the vapour sensing process was saved as an .lvm file. “ ”

C.2. Future Improvements

Bibliography

- [1] J. A. M. J. Frisch and G. W. Trucks and H. B. Schlegel and G. E. Scuseria and M. A. Robb and J. R. Cheeseman and G. Scalmani and V. Barone and G. A. Petersson and H. Nakatsuji and X. Li and M. Caricato and A. V. Marenich and J. Bloino and B. G. Janesko and R. G, J. E. Peralta, F. Ogliaro, et al. *Gaussian ^16 Revision C.01.* 2016.
- [2] R. J. Chen, Y. Zhang, D. Wang, et al. “Noncovalent sidewall functionalization of single-walled carbon nanotubes for protein immobilization”. In: *Journal of the American Chemical Society* 123.16 (2001), pp. 3838–3839. ISSN: 00027863. DOI: 10.1021/ja010172b. URL: <http://pubs.acs.org..>
- [3] Lakshmi N. Cella, Pablo Sanchez, Wenwan Zhong, et al. “Nano aptasensor for Protective Antigen Toxin of Anthrax”. In: *Analytical Chemistry* 82.5 (Mar. 2010), pp. 2042–2047. ISSN: 00032700. DOI: 10.1021/ac902791q. URL: <https://pubs.acs.org/doi/full/10.1021/ac902791q>.
- [4] Rui Campos, Jérôme Borme, Joana Rafaela Guerreiro, et al. “Attomolar label-free detection of dna hybridization with electrolyte-gated graphene field-effect transistors”. In: *ACS Sensors* 4.2 (Feb. 2019), pp. 286–293. ISSN: 23793694. DOI: 10.1021/acssensors.8b00344. URL: <https://pubs.acs.org/doi/full/10.1021/acssensors.8b00344>.
- [5] Han Yue Zheng, Omar A. Alsager, Bicheng Zhu, et al. “Electrostatic gating in carbon nanotube aptasensors”. In: *Nanoscale* 8.28 (July 2016), pp. 13659–13668. ISSN: 20403372. DOI: 10.1039/c5nr08117c. URL: <https://pubs.rsc.org/en/content/articlehtml/2016/nr/c5nr08117c%20https://pubs.rsc.org/en/content/articlelanding/2016/nr/c5nr08117c>.
- [6] Yasuhide Ohno, Kenzo Maehashi, and Kazuhiko Matsumoto. “Label-free biosensors based on aptamer-modified graphene field-effect transistors”. In: *Journal of the American Chemical Society* 132.51 (Dec. 2010), pp. 18012–18013. ISSN: 00027863. DOI: 10.1021/ja108127r. URL: <https://pubs.acs.org/doi/full/10.1021/ja108127r>.
- [7] Xue V. Zhen, Emily G. Swanson, Justin T. Nelson, et al. “Noncovalent monolayer modification of graphene using pyrene and cyclodextrin receptors for chemical sensing”. In: *ACS Applied Nano Materials* 1.6 (June 2018), pp. 2718–2726. ISSN: 25740970. DOI: 10.1021/ACSANM.8B00420/ASSET/IMAGES/LARGE/AN-2018-00420J_0004.JPG. URL: <https://pubs.acs.org/doi/full/10.1021/acsanm.8b00420>.

Bibliography

- [8] Malkom Hinnemo, Jie Zhao, Patrik Ahlberg, et al. “On Monolayer Formation of Pyrenebutyric Acid on Graphene”. In: *Langmuir* 33.15 (Apr. 2017), pp. 3588–3593. ISSN: 15205827. DOI: 10.1021/ACS.LANGMUIR.6B04237/ASSET/IMAGES/LARGE/LA-2016-04237V_0003.JPG. URL: <https://pubs.acs.org/doi/full/10.1021/acs.langmuir.6b04237>.
- [9] Kenzo Maehashi, Taiji Katsura, Kagan Kerman, et al. “Label-free protein biosensor based on aptamer-modified carbon nanotube field-effect transistors”. In: *Analytical Chemistry* 79.2 (Jan. 2007), pp. 782–787. ISSN: 00032700. DOI: 10.1021/ac060830g. URL: <https://pubs.acs.org/doi/full/10.1021/ac060830g>.
- [10] Cristina García-Aljaro, Lakshmi N. Cella, Dhamanand J. Shirale, et al. “Carbon nanotubes-based chemiresistive biosensors for detection of microorganisms”. In: *Biosensors and Bioelectronics* 26.4 (Dec. 2010), pp. 1437–1441. ISSN: 09565663. DOI: 10.1016/j.bios.2010.07.077.
- [11] Basanta K. Das, Chaker Tlili, Sushmee Badhulika, et al. “Single-walled carbon nanotubes chemiresistor aptasensors for small molecules: Picomolar level detection of adenosine triphosphate”. In: *Chemical Communications* 47.13 (Mar. 2011), pp. 3793–3795. ISSN: 1364548X. DOI: 10.1039/c0cc04733c. URL: <https://pubs.rsc.org/en/content/articlehtml/2011/cc/c0cc04733c%20https://pubs.rsc.org/en/content/articlelanding/2011/cc/c0cc04733c>.
- [12] Deana Kwong Hong Tsang, Tyler J. Lieberthal, Clare Watts, et al. “Chemically Functionalised Graphene FET Biosensor for the Label-free Sensing of Exosomes”. In: *Scientific Reports* 9.1 (Sept. 2019), pp. 1–10. ISSN: 20452322. DOI: 10.1038/s41598-019-50412-9. URL: <https://www.nature.com/articles/s41598-019-50412-9>.
- [13] Gregory R. Wiedman, Yanan Zhao, Arkady Mustae, et al. “An Aptamer-Based Biosensor for the Azole Class of Antifungal Drugs”. In: *mSphere* 2.4 (Aug. 2017). ISSN: 23795042. DOI: 10.1128/mSphere.00274-17. URL: [/pmc/articles/PMC5566834/](https://pmc/articles/PMC5566834/)?report=abstract%20https://www.ncbi.nlm.nih.gov/pmc/articles/PMC5566834/.
- [14] Zhaoli Gao, Han Xia, Jonathan Zauberman, et al. “Detection of Sub-fM DNA with Target Recycling and Self-Assembly Amplification on Graphene Field-Effect Biosensors”. In: *Nano Letters* 18.6 (June 2018), pp. 3509–3515. ISSN: 15306992. DOI: 10.1021/acs.nanolett.8b00572. URL: <https://pubs.acs.org/doi/full/10.1021/acs.nanolett.8b00572>.
- [15] Nikita Nekrasov, Natalya Yakunina, Averyan V. Pushkarev, et al. “Spectral-phase interferometry detection of ochratoxin a via aptamer-functionalized graphene coated glass”. In: *Nanomaterials* 11.1 (Jan. 2021), pp. 1–10. ISSN: 20794991. DOI: 10.3390/nano11010226. URL: <https://www.mdpi.com/2079-4991/11/1/226/htm>%20https://www.mdpi.com/2079-4991/11/1/226

- [16] Michael T. Hwang, B. Landon Preston, Lee Joon, et al. “Highly specific SNP detection using 2D graphene electronics and DNA strand displacement”. In: *Proceedings of the National Academy of Sciences of the United States of America* 113.26 (June 2016), pp. 7088–7093. ISSN: 10916490. DOI: 10.1073/pnas.1603753113. URL: <https://www.pnas.org/doi/abs/10.1073/pnas.1603753113>.
- [17] Mohd Maidin Nur Nasyifa, A. Rahim Ruslinda, Nur Hamidah Abdul Halim, et al. “Immuno-probed graphene nanoplatelets on electrolyte-gated field-effect transistor for stable cortisol quantification in serum”. In: *Journal of the Taiwan Institute of Chemical Engineers* 117 (Dec. 2020), pp. 10–18. ISSN: 18761070. DOI: 10.1016/j.jtice.2020.12.008.
- [18] Murat Kuscu, Hamideh Ramezani, Ergin Dinc, et al. “Graphene-based Nanoscale Molecular Communication Receiver: Fabrication and Microfluidic Analysis”. In: (June 2020). arXiv: 2006.15470. URL: <https://arxiv.org/abs/2006.15470v2>.
- [19] Shicai Xu, Jian Zhan, Baoyuan Man, et al. “Real-time reliable determination of binding kinetics of DNA hybridization using a multi-channel graphene biosensor”. In: *Nature Communications* 8.1 (Mar. 2017), pp. 1–10. ISSN: 20411723. DOI: 10.1038/ncomms14902. URL: <https://www.nature.com/articles/ncomms14902>.
- [20] Niazul I. Khan, Mohammad Mousazadehkasin, Sujoy Ghosh, et al. “An integrated microfluidic platform for selective and real-time detection of thrombin biomarkers using a graphene FET”. In: *Analyst* 145.13 (June 2020), pp. 4494–4503. ISSN: 13645528. DOI: 10.1039/d0an00251h. URL: <https://pubs.rsc.org/en/content/articlehtml/2020/an/d0an00251h%20https://pubs.rsc.org/en/content/articlelanding/2020/an/d0an00251h>.
- [21] T Ono, K Kamada, R Hayashi, et al. “Lab-on-a-graphene-FET detection of key molecular events underpinning influenza 2 virus infection and effect of antiviral drugs 3 Running title: Graphene-FET detects reactions in an influenza infection MAIN TEXT”. In: *bioRxiv* (Mar. 2020), p. 2020.03.18.996884. DOI: 10.1101/2020.03.18.996884. URL: <https://doi.org/10.1101/2020.03.18.996884>.
- [22] 6 Pyo Kim, Byung Yang Lee, Joohyung Lee, et al. “Enhancement of sensitivity and specificity by surface modification of carbon nanotubes in diagnosis of prostate cancer based on carbon nanotube field effect transistors”. In: *Biosensors and Bioelectronics* 24.11 (July 2009), pp. 3372–3378. ISSN: 09565663. DOI: 10.1016/j.bios.2009.04.048. URL: <https://pubmed.ncbi.nlm.nih.gov/19481922/>.
- [23] Jagriti Sethi, Michiel Van Bulck, Ahmed Suhail, et al. “A label-free biosensor based on graphene and reduced graphene oxide dual-layer for electrochemical determination of beta-amyloid biomarkers”. In: *Microchimica Acta* 187.5 (May 2020), pp. 1–10. ISSN: 14365073. DOI: 10.1007/s00604-020-04267-x. URL: <https://link.springer.com/article/10.1007/s00604-020-04267-x>.

Bibliography

- [24] Ryan J. Lopez, Sofia Babanova, Kateryna Artyushkova, et al. “Surface modifications for enhanced enzyme immobilization and improved electron transfer of PQQ-dependent glucose dehydrogenase anodes”. In: *Bioelectrochemistry* 105 (Oct. 2015), pp. 78–87. ISSN: 1878562X. DOI: 10.1016/j.bioelechem.2015.05.010. URL: <https://pubmed.ncbi.nlm.nih.gov/26011132/>.
- [25] Guinevere Strack, Robert Nichols, Plamen Atanassov, et al. “Modification of carbon nanotube electrodes with 1-pyrenebutanoic acid, succinimidyl ester for enhanced bioelectrocatalysis”. In: *Methods in Molecular Biology* 1051 (2013), pp. 217–228. ISSN: 10643745. DOI: 10.1007/978-1-62703-550-7_14. URL: <https://pubmed.ncbi.nlm.nih.gov/23934807/>.
- [26] MicroChemicals. *Photoresists AZ and MicroChemicals TI resists*. URL: <https://www.microchemicals.com/products/photoresists.html> (visited on 2023-06-09).
- [27] *SU-8 2000 Permanent Negative Epoxy Photoresist / Kayaku*. URL: <https://kayaku.uam.com/products/su-8-2000/> (visited on 2023-06-30).
- [28] Ziyu Chen and Jeong Bong Lee. “Biocompatibility of SU-8 and Its Biomedical Device Applications”. In: *Micromachines* 2021, Vol. 12, Page 794 12.7 (July 2021), p. 794. ISSN: 2072-666X. DOI: 10.3390/MI12070794. URL: <https://www.mdpi.com/2072-666X/12/7/794/htm%20https://www.mdpi.com/2072-666X/12/7/794>.